International Journal of Mechanical, Industrial and Aerospace Sciences
ISSN: 2517-9950
Vol:6, No:8, 2012

Vortex Wake Formation and Its Effects on Thrust and Propulsive Efficiency of an Oscillating Airfoil

Ahmet Selim Durna, Bayram Celik, Aydin Misirlioglu

***Abstract*—**Flows over a harmonically oscillating NACA 0012 airfoil are simulated here using a two-dimensional, unsteady, incompressibleNavier-Stokes solver.Both pure-plunging and pitching-plunging combined oscillations are considered at a Reynolds number of 5000. Special attention is paid to the vortex shedding and interaction mechanism of the motions. For all the simulations presented here, the reduced frequency (k) is fixed at a value of 2.5 and plunging amplitude (h) is selected to be in the range of 0.2-0.5. The simulation results show that the interaction mechanism between the leading and trailing edge vortices has a decisive effect on the values of the resulting thrust and propulsive efficiency.

***Keywords*—**pithing and plunging airfoil, leading edge vortex, trailing edge vortex, vortex interaction, wake structure.[1]

I. Introduction

THE effective flight capabilities of birds and insects have inspired researchers and engineers to design aircrafts utilizing flapping mechanism for ages. Recently, flapping wing aerodynamics has generated a great deal of interest due to the increased design efforts of Micro Air Vehicles (MAV) and rapidprogressin computer capabilities [1]. MAV's are defined as flying vehicles having wingspan no longer than 15 cm and a flight speed in the range of 10-20 km/h [2]. Because of aroused interest in MAV, there are number of studies on flapping airfoils, and the generated thrust and lift. In nature, the flapping mechanism of a flying animal is a combination of pitching, plunging, and sweeping motions. Researchers carry out two dimensional analyses to understand the underlying physics of the flapping mechanisms before extending their study into the three dimensional analysis and the combined motion.

Thrust generation with oscillating airfoils has been known since the first recorded studies by Knoller [3] and Betz[4]. These studies showed that an insect had an ability to generate a propulsive force by its oscillating wings. Karman and Burgers [5] provided the first theoretical explanation for this type of drag and thrust production and their relation with the location, and orientation of the wake vortices

Taylor et al. [6] have shown a wide variety of animals operating within a narrow band of Strouhal number that is in the range of 0.2 and 0.4.

1. AhmetSelimDurna is graduate student at the Istanbul Technical University, 34469 Turkey. (phone: +90 0 212 285 31 22; e-mail: durnaa@itu.edu.tr)
2. BayramCelik is assistant professor at the Department of Astronautical Engineering, Istanbul Technical University, 34469 Turkey (e-mail:celikbay@itu.edu.tr)
3. AydinMisirlioglu is professor at the Department of Astronautical Engineering, Istanbul Technical University, 34469, Turkey (e-mail: misirli@itu.edu.tr).

The Strouhal number is defined as

$$St = fA/U_\infty \quad (1)$$

where*f, A,*and U_∞ denote the flapping frequency (in Hertz), wake width, and flight speed, respectively. Platzer et al. [1] show that the Strouhal number range of 0.2-0.4 reported in Taylor's study is equivalent to a reduced frequency (k) times plunging amplitude (h) range of 0.3-0.6 for a pure-plunging motion.

Jones et al. [7], and Lai and Platzer [8] utilized a flow visualization method for an oscillating NACA0012 airfoil to illustrate the wake vortex patterns under various reduced frequencies, *k.* The harmonic motion of the airfoil generates vortices shedding from the leading and trailing edges. The interaction between the vortices, and flow kinematics result in a formation of pattern of large-scale eddies were shown in the study of Koochesfahani[9], Oshima&Natsume and Anderson[7,10]. Young and Lai, Percin[11-13] showed variation of propulsive efficiency versus *kh* values. They observed that propulsive efficiency reached a peak, and then started to decrease as the *kh*was increased. Although, there have been numerous studies on the effects of the plunging amplitude, frequency, thrust coefficient, and propulsive efficiency, the studies focusing on the vortex interaction mechanism are limited. The vortex dynamics of flapping MAV is crucial in terms of to determine the appropriate configuration and to understand the flight characteristics.

The main objective of present study is to understand theformation and interaction mechanisms of the vortices shedding from the leading and the trailing edges of an airfoil in pure-plunging and pitching-plunging combined motions.

II. Description of the Model

A. Kinematics

In this study, two different types of simple harmonic motion are considered for NACA 0012. While the first one consists of pure plunging, the second one is a combination of pitching and plunging. The pitchingtakes place about a pivot point at a quarter chord behind the leading edge. In order to simulate the plunging motion of the airfoil as well as the mesh movement, the following expression is used:

$$y(t) = h \sin(\omega t) \quad (2)$$

where h is the dimensionless plunging amplitude (normalized with chord), ω is the angular frequency, and y is the instantaneous position of the airfoil center. For the pitching, the rotational motion is expressed as

$$\alpha(t) = \alpha_0 + \alpha_{max}\sin(\omega t + \varphi) \quad (3)$$

where α_0 is the initial angle of attack, α_{max} is the maximum value of the pitching amplitude, φ is the phase lag between plunging and pitching motions. For combined case, these translational and rotational motions are simulated together. The motion of the boundaries and the mesh in the computational domain due the oscillating airfoil are handled here by hooking a User DefinedFunction (UDF).

B. Grid Generation

The selection of an appropriate grid topology and its generation is an essential part of any CFD process. In this study, the generated C type mesh consists of 111880 quadrilateral cells. The left and right outer boundaries of the computational domain are located at 20 and 15 chords away from the airfoil in the downstream and upstream directions, respectively. The top and bottom boundaries are 15 chords away from the airfoil. (see Fig. 1). The first grid point next to the airfoil is chosen to be located at 10^{-3} chord length distance in the direction normal to the surface.

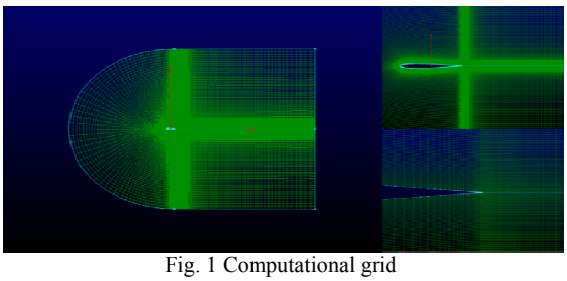

Fig. 1 Computational grid

In order to reduce computational time without compromising the numerical accuracy, grid independence test and time step refinementwere carried out. Two different C-type structural meshes with total elements of 111880 and 225900 were generated for grid independence study. The meshes arevery fine near the airfoil and they are getting coarser in the direction of normal to the airfoil surface.(see Fig. 1). Comparisons of the peak values of C_l and C_d obtained by using these two different meshes show that the discrepancy is lessthan 1%. Variation of C_d in time is shown in Fig. 2 for 3 different time step sizes (Δt), namely 1/500, 1/1000, and 1/2000 of a plunging period. In the figure, the time step sizes are normalized with the plunging period, T.As can be seen from the figure, even the largest step sizecould be used for the simulation.The study shows that the change in the peakvalue of C_l and C_d are less than 1%.

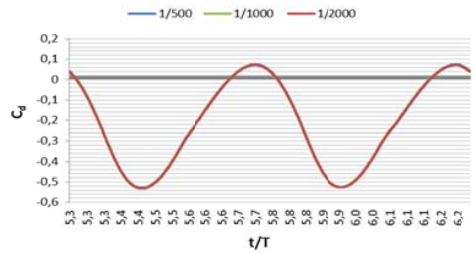

Fig. 2 Time history of thrust coefficient for3 different time-step sizes

C. Numerical Analysis

The unsteady flow field around an oscillating airfoil is simulated using a two dimensional, incompressible Finite Volume Navier-Stokes solver. The features of the commercial code FLUENT version 6.3.26, such as the second order upwind for spatial discretization and first order time accuracy allow us to simulate unsteady flow field around the airfoil. The coupling between the pressure and the velocity is achieved by means of the PISO algorithm. The PISO algorithm is generally efficient for the transient flow computation. It is assumed that the flow is laminar at Reynolds number (Re = 5000).The dynamic mesh technique is employed to model the motion of the airfoil (rigid-body motion).

D.Forces and power

The thrust coefficient, C_t, and propulsive efficiency,η are used by outputs for all cases. The propulsive efficiency of an airfoil is defined as the ratio of the propulsive power to the input power, which are given below with Equations 4 and 5, respectively.

$$C_{tmean} = -\frac{1}{T}\int_t^{t+T} C_d(t)dt \quad (4)$$

$$C_{pmean} = -\frac{1}{T}\int_t^{t+T}\left[\frac{C_l(t)\dot{y}(t)}{c} + C_m(t)\dot{\theta}(t)\right]dt \quad (5)$$

The propulsive power of an airfoil is generated by the thrust force. Therefore, the propulsive efficiency is expressed by

$$\eta = \frac{C_{tmean}}{C_{pmean}} \quad (6)$$

whereC_d, C_l and C_m are the drag, lift and moment coefficients.$\dot{y}(t)$and$\dot{\theta}(t)$ are translational (plunging) and angular displacement rate, respectively.

III. Results and Discussions

We performed simulations for pure-plunging and pitching and plunging motions. The reduced frequency (k) was fixed at a value of 2.5, and the plunging amplitude (h) was selected to be in the range of 0.2 to 0.5 for all motions.

A. Pure-plunging motion

We examined the time histories of the thrust and lift coefficients for various plunging amplitudes at constant frequency.

As a result of symmetries of the airfoil and its motion, it is expected that time history of the lift coefficient, C_l symmetrically oscillates about the zero. However, as can be seen from Fig. 3, the lift coefficients' histories have prominent for h >2. In order to understand the exact mechanism behind this observation, it is essential to focus on the vortex dynamics resulted from the oscillating airfoil.

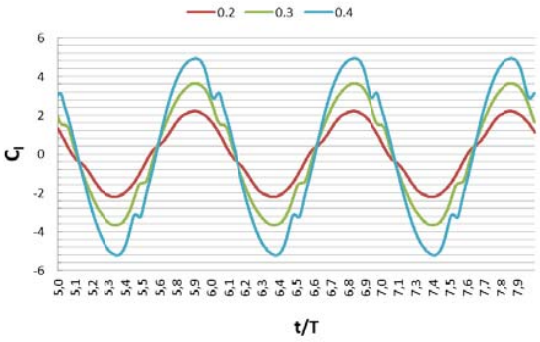

Fig. 3 Time histories of lift coefficients for h=0.2, 0.3 and 0.4.

The thrust coefficient, C_t has the same magnitude but opposite sign of the drag coefficient, C_d. On the contrary of the time history of the lift coefficient shown in Fig. 3, the time history of the trust coefficients show an asymmetry about the zero axis (see Fig. 4). In addition to this discrepancy, as the oscillation amplitude, h increases, mean of the thrust coefficient rises.While the thrust is generated in both upward and downward motion of the body, the lift is generated only during the downward motion. Therefore, the period of the thrust coefficient is twice the period of lift coefficient.

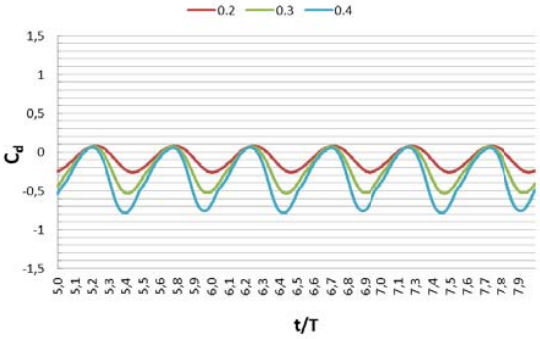

Fig. 4 Time histories of thrust coefficients for h=0.2, 0.3 and 0.4.

For h = 0.2, the formation of vortices and their interactions are shown in Fig. 5. As can be seen from this figure, a period of the movement is represented by 8 different snapshots with a time increment of t/T = 0.125. In this figure, positive (counter-clockwise rotating) and negative (clockwise rotating)vorticesare represented by blue and red color, respectively.

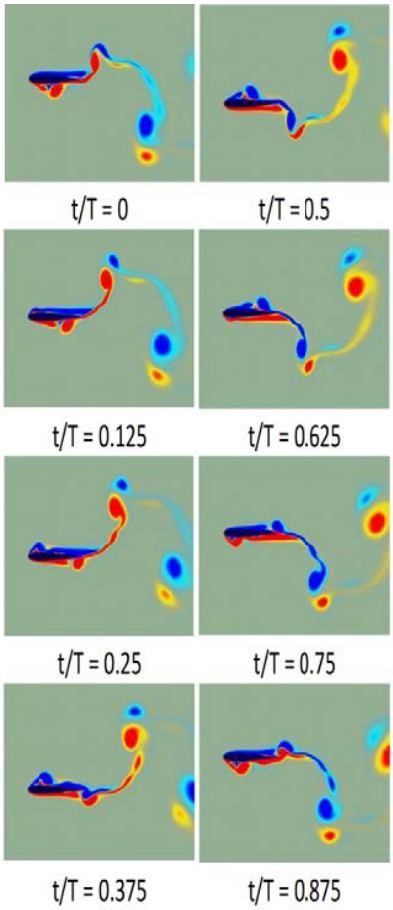

Fig. 5 Vorticity contour snapshots of a NACA 0012 airfoil plunging with an amplitude of h=0.2

When the airfoil starts to move downward (t/T = 0.0), a counter-clockwise rotating leading edge vortex (LEV) starts to form on the lower side of the airfoil. Then, the LEV is convected to the trailing edge as the airfoil continues to move downward (t/T = 0.125 - 0.375). When the airfoil starts to move upward (t/T = 0.5), the clockwise vorticity field resulted from the boundary layer formed on the upper side of the airfoil transforms into a trailing edge vortex (TEV). The LEV and the TEV form a counter rotating vortex pair, which is convected away from the airfoil for t/T> 0.5.

The vorticity contour snapshots for h = 0.3 are shown in Fig. 6, where the instants are in the same sequence as in the previous figure. As can be seen from the figure, the counter-clockwise rotating LEV is wrapped with a clockwise rotating vortex while the LEV is convected along the lower side of the airfoil (t/T = 0.125-0.375). Then, this relatively weak additional vortex and TEV diffuses quicker than the LEV as they are convected away from the airfoil (t/T> 0.5).

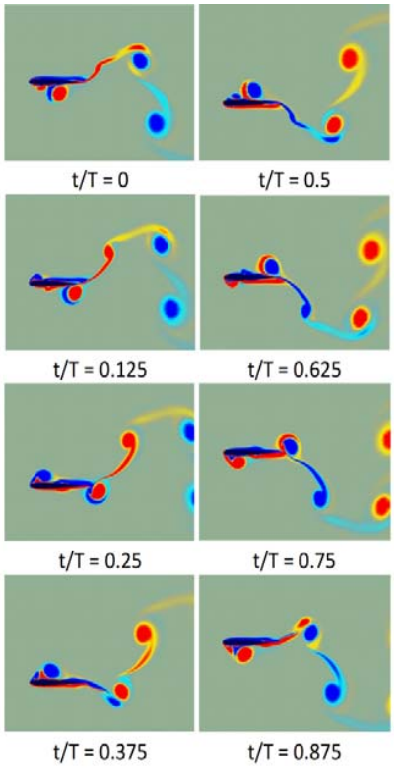

Fig. 6 Vorticity contours for h=0.3 at an instants of t/T=0-1.0

Similar to the previous two figures, the vorticity contour snapshots for h = 0.4 are shown in Figure 7. Comparison of the 3 sets of instants given in Fig. 6-7 shows that as the plunging amplitude h increases, relatively higher intensities are considered for all the three vortices, namely LEV, TEV and the additional vortex. Moreover, an increase in plunging amplitude makes the additional vortex stronger, and thereby the prominent observed in the histories of the lift coefficient becomes apparent for h> 0.3.

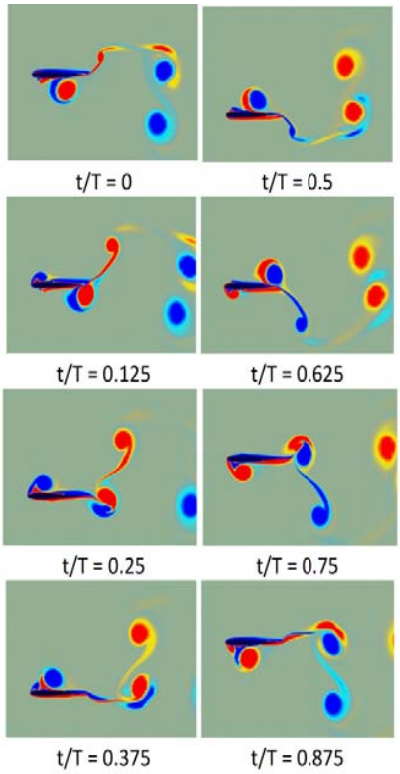

Fig. 7 Vorticity contours for h=0.4 at an instants of t/T=0-1.0

In order to see the effects of oscillating amplitude on vortex structure, the vorticity contours of the flows with h=0.2, 0.3, and 0.4 are given in Fig. 8 for comparison. In this figure, all the snapshots show an instant of t/T=0.0.

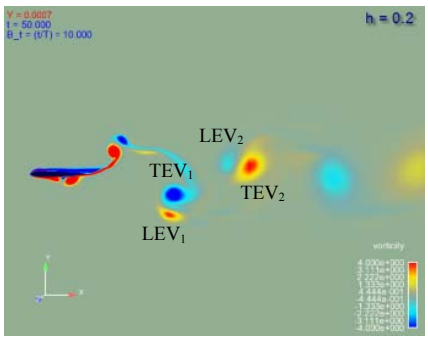

h=0.2

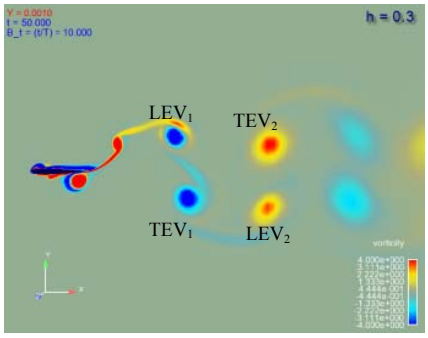

h=0.3

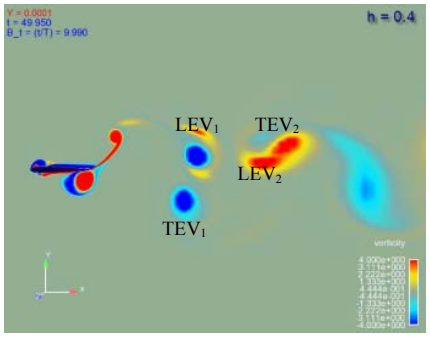

h=0.4

Fig. 8 Vortex formations according to plunging amplitude

It is obvious from the figure that as the *h* increases the vortices shed from the airfoil get higher intensities. However, as the *h* increases, the LEV gains relatively higher streamwise velocity in comparison to the TEV. This discrepancy generates totally different downstream vortex pattern. For example, while the LEV is behind the same signed TEV for $h = 0.2$, the LEV appears in front of the same signed TEV for $h = 0.4$. Moreover, the distance between the two vortices in the direction of normal to the flow gets shorter as *h* increases. As a result, these two vortices coalescence and diffuse in the downstream of the flow for $h = 0.4$. We also observed that an increase in the plunging amplitude beyond 0.4 caused disorder in periodicity of vortex structure and generated more complex thrust and lift coefficient histories. In order to make a smooth operation of MAV and to be able to control it easily, periodic force generation and vortex structure are desired.

Fig 9 shows the variations of thrust coefficient and propulsive efficiency vs. plunging amplitude. It can be seen that C_t increases linearly with plunging amplitude. On the other hand, propulsive efficiency shows a linear increase up to $h = 0.25$ and then reaches a plateau after h=0.3. We observed that there is a disorder in the periodicity beyond the plunging amplitude value of 0.4. This observation is supported by the Young and Lai's study [13] which says η starts to decrease after a plateau.

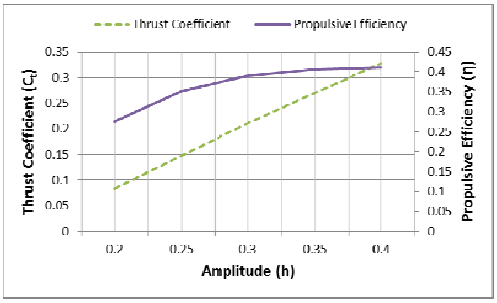

Fig. 9 Thrust coefficient and propulsive efficiency vs. plunging amplitude

B. Combined pitching and plunging motion

The kinematics of the flow resulted from the combined motion of the airfoil is investigated at a fixed pitching amplitude of $\alpha_{max} = 10^o$by varying the plunging amplitude 0.2 through 0.4. The value of the phase lag between the pitching and plunging is kept constant to be φ=90°

For $h = 0.2$, the formation of vortices and their interactions are shown in Fig. 10. In the figure,the instants are in the same sequence as given in the Figures 5-7. As can be seen from the figure, during the upward ($t/T < 0.5$) and downward ($t/T > 0.5$) motions of the airfoil, counter-clockwise and clockwise rotating TEV's are formed, respectively. Apart from the pure plunging cases, the pitching mechanism weakens the LEV formation here. The relatively weak LEV's diffuse easily after interacting with the TEV's. As result of the pitching mechanism, TEV dominant downstream vortex patterns are considered here.

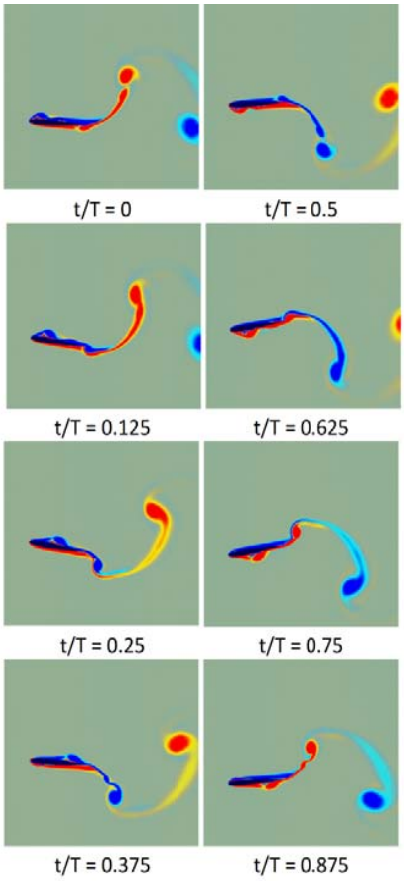

Fig. 10 Vorticity contour snapshots of a NACA 0012 airfoil plunging and pitching with an amplitude of h=0.2 and $\alpha_{max} = 10°$

In Fig. 11, the vorticity contour snapshots of combined motion with$h$=0.3 are shown. In contrary to the case with h= 0.2 shown in Fig.10, the increased plunging amplitude generates clockwise and counter clockwise rotating LEV's during the upward and downward motions of the airfoil, respectively. In addition to the LEV's, counter rotating additional vortices are formed (see the instants t/T= 0.125 and 0.625).Apart from the pure plunging case shown in Fig. 7., strong interactions between the TEV and the shear layer formed on the other side of the airfoil is considered at the instants of t/T= 0.25 and 0.75. This interaction causes shedding of more than two vortex cores at each stroke.

However, the weaker vortices diffuse later and the same signed LEV-TEV pair is convected by the freestream. The TEV is stronger than the LEV here.

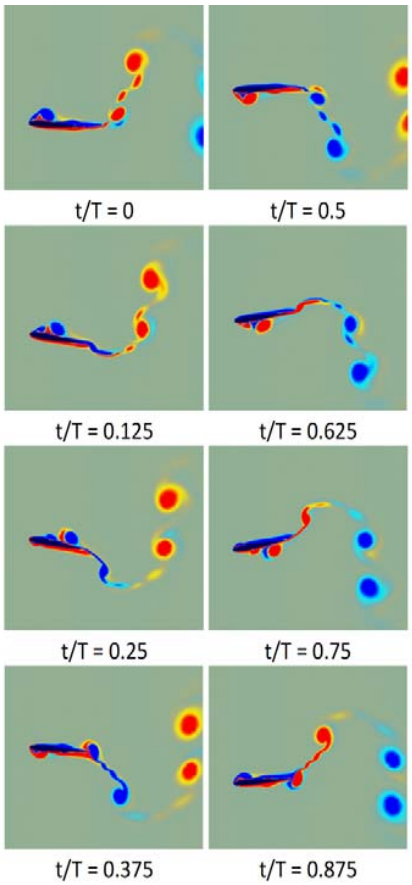

Fig. 11 Vorticity contour snapshots of a NACA 0012 airfoil pitching and plunging atan amplitude of$\alpha_{max} = 10°$ and *h*=0, respectively

The vorticity contours of the combined motion with *h*=0.4 are shown in Fig. 12. Although the vortex shedding mechanism is very similar to the case with *h*=0.3, downstream vortex patterns are quite different. This discrepancy is resulted from appearance of relatively stronger shear layers formed on the two sides of the airfoil. While one of these shear layer extends from the airfoil and feeds the TEV, the other with opposite signed cuts this extending layer more than once. This mechanism forms more than 2 vortex cores in addition to the LEV and TEV, and they do not diffuse quickly. Later, the LEV catches the TEV and coalescence of them forms a relatively bigger single core in downstream. In comparison to pure plunging case with *h*= 0.4, combined motion weakens the LEV and additional vortices but reduces the time taken to merge of the LEV and TEV

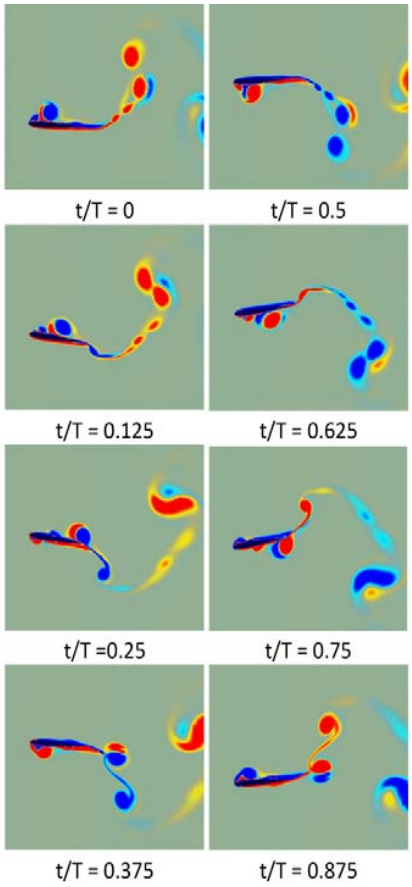

Fig. 12 Vorticity contour snapshots of a NACA 0012 airfoil plunging and pitching with an amplitude of h=0.4 and $\alpha_{max} = 10°$

IV. Conclusions

The wake structure and corresponding force coefficients of a NACA 0012 airfoil in pure-plunging and pitching-plunging combined motions have been studied here. In pure-plunging motion, there is only TEV at small plunging amplitudes ($h \leq 0.2$) but there are both LEV and TEV at large amplitudes ($h \geq 0.3$). It is seen that the developed LEV has a major influence on the wake region such as formation of Karman Vortex Street. In addition to vortex structure, we have examined the effect of the amplitude on force coefficients. The thrust increases linearly with increasing amplitude and propulsive efficiency reaches a maximum value at about the plunging amplitude of 0.35. Moreover, increasing the plunging amplitude can take the airfoil from drag generating to thrust generating. In combined motion, the pitching mechanism weakens the LEV and the additional vortices. Pitching-plunging combined motion introduces relatively complex vortex formation mechanism and vortex interaction. Although the vortex dynamics of the simulated cases are analyzed here, there is a need to extend this study to cover wider ranges of pitching amplitude and phase lag.

Acknowledgment

The first author is grateful for the financial support provided by Istanbul Technical University (ITU).

REFERENCES

[1] S. Buckingham, "Three-Dimensional Computational Analysis of the Flow Around an Oscillating Flat Plate", Graduate Thesis, Istanbul Technical University, 2009.
[2] C.M.S.F. James M. McMichael, Micro Air Vehicles - Toward a New Dimension in Flight, 1997.
[3] R. Knoller, Flüssigkeitswiderstand und Propellertheorie, Verlag des Österr. flugtechnischen Vereines, Wien,, 1909, p. 32.
[4] A. Betz, Ein Beitrag zur Erklärung des Segelfluges, Jan. 1912.
[5] T.a.B. Von Karman, J. M., General Aerodynamic Theory - Perfect Fluids, 1943.
[6] G.K. Taylor, R.L. Nudds, A.L.R. Thomas, Nature, Vol. 425, 2003,pp. 707-711.
[7] J.M. Anderson, K. Streitlien, D.S. Barrett, M.S. Triantafyllou, Journal of Fluid Mechanics 360, 1998,pp. 41-72.
[8] J.C.S. Lai, Platzer, M.F., , AIAA Journal,Vol. 39,2001,pp. 531-534
[9] M.M. Koochesfahani, AIAA Journal , Vol. 27, 1989,pp. 1200-1205.
[10] Y. Oshima, Natsume, A.,, Merzkirch W. (Ed.),1980,pp. 295-299.
[11] M.F. Platzer, K.D. Jones, J. Young, J.C.S. Lai, AIAA Journal, Vol. 46, 2008,pp. 2136-2149.
[12] Perçin,M., Mısırlıoğlu, A., Ünal, M.F., Flow Around A Plunging Airfoil In A Uniform Flow, in: AIAC, Ankara, Turkey, 2009, No. 46.
[13] Young, J. and Lai, J.C.S., Mechanisms Influencing the Efficiency of Oscillating Airfoil Propulsion, AIAA Journal, Vol. 45, No. 7, 2007, pp. 1695-1702.